



<b>Title</b>	<b>Theoretical and experimental study of plate-strengthened concrete columns under eccentric compression loading</b>
<b>Author(s)</b>	<b>Wang, L; Su, KL</b>
<b>Citation</b>	<b>Journal of Structural Engineering, 2013, v. 139 n. 3, p. 350-359</b>
<b>Issued Date</b>	<b>2013</b>
<b>URL</b>	<b><a href="http://hdl.handle.net/10722/185745">http://hdl.handle.net/10722/185745</a></b>
<b>Rights</b>	<b>Journal of Structural Engineering-ASCE. Copyright © American Society of Civil Engineers.</b>

# Theoretical and Experimental Study of Plate-Strengthened Concrete Columns under Eccentric Compression Loading

Lu Wang<sup>1</sup>, Ray Kai-Leung Su<sup>2</sup>

## Abstract

Steel jacketing has been widely used for strengthening reinforced concrete (RC) columns in the past four decades. In practice, the RC columns to be strengthened are usually subjected to eccentric pre-compressed axial loads. Until now, there have been only limited studies conducted that address the stress-lagging effects between the original column and the new jacket due to the pre-existing load. In this paper, the precambered steel plate strengthening approach, which can alleviate the stress-lagging effects, was adopted to improve the axial strength and moment capacity of the preloaded RC columns subjected to eccentric compression loading. An experimental study that involved eight specimens with different eccentricities, plate thicknesses and initial precamber displacements was conducted to examine the ductility and moment-curvature response of strengthened columns and to validate the effectiveness of this approach. A theoretical model was developed to predict the axial load capacity of the plate-strengthened columns. A comparison of the theoretical and experimental results showed that the theoretical model accurately predicted the axial load-carrying capacities of the plate-strengthened columns under eccentric compression loading.

## Keywords:

Reinforced Concrete Columns; Precambered Steel Plates; Strengthening; Eccentric Loads

<sup>1</sup> PhD Candidate, Dept. of Civil Engineering, The Univ. of Hong Kong, Pokfulam Rd., Hong Kong, E-mail: wanglu@hku.hk

<sup>2</sup> Associate Professor, Dept. of Civil Engineering, The Univ. of Hong Kong, Pokfulam Rd., Hong Kong, corresponding author. E-mail: klsu@hkucc.hku.hk

## 27 **Introduction**

28 Due to the deterioration of materials and the demand for additional strength, a large number of  
29 reinforced concrete (RC) columns may need to be retrofitted or strengthened. Steel jacketing, which is  
30 executed by attaching steel plates or angles onto the concrete, has been widely used to strengthen RC  
31 structures due to the cost effectiveness and simple construction. Although a number of studies (Oey et  
32 al. 1996; Ersoy et al. 1993; Ramírez 1996; Wu et al. 2006; Fukuyama et al. 2000; Cirtek et al. 2001;  
33 Adam et al. 2007, 2008 and 2009; Giménez et al. 2009) were conducted to investigate the performance  
34 of the jacketed columns under axial compression loads, only a few considered the effects of pre-  
35 existing loads on stress-lagging between the concrete core and the new jacket. Ersoy et al. (1993),  
36 Takeuti et al. (2008) and Giménez et al. (2009) experimentally investigated the effects of pre-existing  
37 loads on the strengthening efficiency. Their test results demonstrated that the stress-lagging effects can  
38 significantly decrease the ultimate axial load capacity of the strengthened columns.

39 In real applications, many columns are subjected to various degrees of eccentric compression  
40 loading. The effects of RC columns strengthened by steel jackets under eccentric compression loads  
41 should be investigated. Li et al. (2009) and Garzón et al. (2011) studied the behavior of steel-caged  
42 columns under combined bending and axial loads. Their experimental results revealed that the steel  
43 strips and angles can increase the load resistance and ductility of strengthened columns. Montuori and  
44 Piluso (2009) tested thirteen RC columns strengthened by steel angles and battens under eccentric  
45 loading. Their study demonstrated that both the axial load-carrying capacity and the lateral  
46 deformability of strengthened concrete columns can be enhanced. Furthermore, they proposed a  
47 theoretical model that was able to predict the load-carrying capacity of the strengthened columns  
48 based on a kinematic mechanism. In their model, the hoops were considered simple support restraints,  
49 and the longitudinal bar was modeled as a continuous beam on simple supports that were subjected to  
50 a compressive axial load. With increasing axial load, the section of the bar between the two hoops  
51 developed a kinematic mechanism characterized by three plastic hinges. In addition, a comparison of  
52 the moment-curvature responses was performed that showed the accuracy of the model in predicting

53 the structural response within the whole deformation range. Our companion paper (Wang and Su 2012)  
54 presented a test of nine preloaded RC columns strengthened by precambered steel plates under  
55 eccentric loading. The test results showed that precambered steel plates could actively share the existing  
56 axial loads with the original column. Stress relief in the original concrete column and post-stress developed  
57 in the steel plates can alleviate the stress-lagging and displacement incompatibility problems. Both the  
58 axial and moment capacities of strengthened columns were enhanced. The post-yield deformation was  
59 substantially increased.

60 In this paper, new experimental results in terms of the ductility and moment-curvature response of  
61 strengthened RC columns with precambered steel plates under eccentric compression loads are  
62 presented. A theoretical model based on elementary structure mechanics with consideration of stress-  
63 lagging effects was developed to predict the axial load-carrying capacity of plate-strengthened  
64 columns under eccentric compression loading. The accuracy of the model was verified through a  
65 comparison of the model with experimental results obtained by the authors and by Montuori and  
66 Piluso (2009).

67

## 68 **Theoretical model**

### 69 ***Initial Precamber***

70 Two stainless steel rods and bolts are used to control the initial deformation of the plates and to form  
71 the required precambered profile as shown in Fig. 1. Because the bolts at both ends of the steel plates  
72 restrain the end rotations of the plates, the initial lateral displacement ( $v$ ) of the precambered plate can  
73 be approximated by a cosine function (Su et al. 2011) as expressed in Eq.(1).

$$74 \quad v = \frac{\delta}{2} \left[ 1 - \cos \left( \frac{2\pi x}{L_{rc,pl}} \right) \right] \quad (1)$$

75 where  $\delta$  is the initial precamber at the mid-height of the plate,  $L_{rc,pl}$  is the clear height of the RC  
76 column under preloading ( $P_{pl}$ ),  $x$  is the coordinate defined along the height of the column, and the

77 subscript  $pl$  denotes the preloading stage. Eq. (1) satisfies the boundary conditions at both ends of the  
 78 steel plates, i.e.,  $v = 0$  and  $\frac{dv}{dx} = 0$  when  $x = 0$  or  $x = L_{rc,pl}$ .

79 The difference in length of the steel plate and the RC column ( $\Delta_L$ ) can be evaluated by Eq. (2).

$$80 \quad \Delta_L = \frac{1}{2} \int_0^{L_{rc,pl}} \left( \frac{dv}{dx} \right)^2 dx \quad (2)$$

81 Putting Eq. (1) into Eq. (2) gives

$$82 \quad \Delta_L = \frac{(\pi\delta)^2}{4L_{rc,pl}} \quad (3)$$

### 83 ***Material Constitutive Laws and Simplified Stress Block Model***

84 The stress-strain relationship of concrete in compression is represented by the parabolic relationship  
 85 proposed by Hognestad et al. (1955).

$$86 \quad \sigma_c = f_c' \left[ \frac{2\varepsilon_c}{\varepsilon_{co}} - \left( \frac{\varepsilon_c}{\varepsilon_{co}} \right)^2 \right] \quad (4)$$

87 where  $f_c'$  is the concrete compressive cylinder strength,  $\sigma_c$  and  $\varepsilon_c$  are the stress and strain of the  
 88 concrete, respectively, and  $\varepsilon_{co}$  is the concrete compressive strain corresponding to  $f_c'$ .

89 Both the steel plates and steel bars are assumed to be elasto-plastic materials. In the initial elastic  
 90 stage, the stress-strain models of steel plates and steel bars can be expressed as

$$91 \quad \sigma_p = E_p \varepsilon_p \quad (5)$$

$$92 \quad \sigma_s = E_s \varepsilon_s \quad (6)$$

93 where  $\sigma_p$  and  $\varepsilon_p$  are the stress and strain of steel plates, respectively, and  $\sigma_s$ ,  $\varepsilon_s$  and  $E_s$  are the stress,  
 94 strain and Young's modulus of the steel bars, respectively.

95 Collins and Mitchell (1987) noted that, for a column section with a constant width, the parabolic  
 96 portion of the concrete stress distribution can be replaced by an equivalent rectangular block by  
 97 introducing the stress block factors  $\alpha$  and  $\beta$  as shown in Fig. 2, which can be calculated using Eq. (7)  
 98 and Eq. (8).

99

$$\alpha = \left[ \frac{\varepsilon_{cu}}{\varepsilon_{c0}} - \frac{1}{3} \left( \frac{\varepsilon_{cu}}{\varepsilon_{c0}} \right)^2 \right] / \beta \quad (7)$$

100

$$\beta = \left( 4 - \frac{\varepsilon_{cu}}{\varepsilon_{c0}} \right) / \left( 6 - \frac{2\varepsilon_{cu}}{\varepsilon_{c0}} \right) \quad (8)$$

### 101 **Preloading stage**

102 The preloading force is resisted by concrete and steel bars before flattening the precambered steel  
103 plates. The equilibrium equation of the RC column before flattening the plates can be obtained from  
104 the sum of the internal forces.

105

$$P_{pl} = \alpha \beta b (c_{pl} - 2d_b) f_c' \left( \frac{2\varepsilon_{c,pl}}{\varepsilon_{c0}} - \frac{\varepsilon_{c,pl}^2}{\varepsilon_{c0}^2} \right) + E_{sc} A_{sc} \varepsilon_{c,pl} \left( \frac{c_{pl} - d'}{c_{pl}} \right) - E_{st} A_{st} \varepsilon_{c,pl} \left( \frac{d - c_{pl}}{c_{pl}} \right) \quad (9)$$

106 The equation obtained from taking moments about the tension steel is

107

$$P_{pl} e' = \alpha \beta b (c_{pl} - 2d_b) f_c' \left( \frac{2\varepsilon_{c,pl}}{\varepsilon_{c0}} - \frac{\varepsilon_{c,pl}^2}{\varepsilon_{c0}^2} \right) \left( d - \frac{\beta c_{pl}}{2} \right) + E_{sc} A_{sc} \varepsilon_{c,pl} \left( \frac{c_{pl} - d'}{c_{pl}} \right) (d - d') \quad (10)$$

108 where  $b$  is the width of the column section as shown in Fig. 2,  $d$  and  $d'$  are the depths of the tension  
109 steel and the compression steel measured from extreme compression fiber, respectively,  $d_b$  is the  
110 diameter of the bolt hole,  $E_{sc}$  and  $E_{st}$  are the Young's moduli of the compression steel bar and tension  
111 steel bar, respectively,  $A_{sc}$  and  $A_{st}$  are the total cross-sectional areas of the compression steel bars and  
112 tension steel bars, respectively, and  $e'$  is the distance between the load point and the tension steel. The  
113 depth of the compression zone ( $c_{pl}$ ) and the concrete strain at extreme compression fibers ( $\varepsilon_{c,pl}$ ) in the  
114 preloading stage can be obtained from Eqs. (7), (8), (9) and (10).

115 The axial stiffness of the RC column ( $K_{rc,pl}$ ) and a steel plate ( $K_p$ ) can be determined by Eq.(11) and  
116 Eq.(12), respectively.

117

$$K_{rc,pl} = \frac{E_c A_c}{L_{rc,pl}} \quad (11)$$

118

$$K_p = \frac{E_p A_p}{L_p} \quad (12)$$

119 where  $E_c$  and  $E_p$  are the values for the Young's moduli of concrete and steel plates, respectively,  $A_c$  is  
120 the cross-sectional area of the RC column considering the cracked section,  $A_p$  is the cross-sectional  
121 area of a steel plate and  $L_p$  is the undeformed length of the steel plate.

122

### 123 ***Post-stressing stage***

124 When the precambered steel plates are flattened, the preloading force is resisted by concrete, steel bars  
125 and steel plates. Fig. 3 shows the lengths and deformations of the plates and the RC column at three  
126 different loading stages, i.e., the undeformed stage, the preloading stage and the post-stressing stage.  
127 By progressively tightening the bolts on both sides of the column, the precambered steel plates are  
128 gradually flattened. Due to the arching action, a post-compressive force ( $P_{p,ps}$ ) is generated in the steel  
129 plates, and an equal magnitude de-compressive force is generated in the RC column. Using Hooke's  
130 law, the total post-stressed force provided by the plates is

$$131 \quad P_{p,ps} = 2K_p \Delta_{p,ps} \quad (13)$$

132 where  $\Delta_{p,ps}$  is the axial shortening of the steel plate while tightening the bolts when compared to the  
133 original undeformed state, and the subscript  $ps$  denotes the post-stressing stage.

134 The de-compressive force in the RC column can be written as

$$135 \quad P_{p,ps} = K_{rc,pl} \Delta_{rc,ps} \quad (14)$$

136 where  $\Delta_{rc,ps}$  is the increase in length of the RC column during the post-stressing stage, as shown in Fig.  
137 3.

138 The difference in lengths of the steel plate and RC column in the preloading stage can be expressed  
139 as

$$140 \quad \Delta_L = L_p - L_{rc,pl} \quad (15)$$

141 According to the displacement compatibility model (Fig. 3), the difference in the lengths of the steel  
142 plate and RC column in the preloading stage is equal to the sum of the axial stretching of the RC  
143 column ( $\Delta_{rc,ps}$ ) and the axial shortening of the steel plates ( $\Delta_{p,ps}$ ). Hence,

$$144 \quad \Delta_L = \Delta_{rc,ps} + \Delta_{p,ps} \quad (16)$$

145 Substituting Eq. (13) and Eq. (14) into Eq. (16) gives

$$146 \quad \Delta_L = \frac{K_{rc,pl} + 2K_p}{K_{rc,pl}} \Delta_{p,ps} \quad (17)$$

147 Putting Eq. (17) into Eq. (13), the post-compressive force in the plates can be obtained by

$$148 \quad P_{p,ps} = \Delta_L \frac{2K_p K_{rc,pl}}{2K_p + K_{rc,pl}} \quad (18)$$

149 Meanwhile, the stress of steel plates ( $\sigma_{p,ps}$ ) at the post-stressing stage can be expressed by

$$150 \quad \sigma_{p,ps} = \frac{P_{p,ps}}{2A_p} \quad (19)$$

151 By considering vertical force equilibrium, the preloading force is resisted by the concrete, the steel  
152 bars and the steel plates. Hence,

$$153 \quad P_{pl} = \sigma_{c,ps} A_c + \sigma_{s,ps} A_s + 2\sigma_{p,ps} A_p \quad (20)$$

154 where  $\sigma_{c,ps}$ ,  $\sigma_{s,ps}$  and  $\sigma_{p,ps}$  are the axial stresses in the concrete, the steel bars and the steel plates in the  
155 post-stressing stage, respectively, and  $A_s$  is the total cross-sectional area of the vertical steel bars.

156 We assume that there is no bond slip between the steel bars and the concrete. Hence,

$$157 \quad \varepsilon_{c,ps} = \varepsilon_{s,ps} \quad (21)$$

158 By considering the equivalent rectangular stress block, the equilibrium equation of the strengthened  
159 column can be obtained from the sum of the internal forces.

$$160 \quad P_{pl} = \alpha\beta b(c_{ps} - 2d_b) f_c' \left( \frac{2\varepsilon_{c,ps}}{\varepsilon_{c0}} - \frac{\varepsilon_{c,ps}^2}{\varepsilon_{c0}^2} \right) + E_{sc} A_{sc} \varepsilon_{c,ps} \left( \frac{c_{ps} - d'}{c_{ps}} \right) - E_{st} A_{st} \varepsilon_{c,ps} \left( \frac{d - c_{ps}}{c_{ps}} \right) + 2A_p \sigma_{p,ps} \quad (22)$$

161 The equation obtained from taking moments about the tension steel is

$$162 \quad P_{pl} e' = \alpha\beta b(c_{ps} - 2d_b) f_c' \left( \frac{2\varepsilon_{c,ps}}{\varepsilon_{c0}} - \frac{\varepsilon_{c,ps}^2}{\varepsilon_{c0}^2} \right) \left( d - \frac{\beta c_{ps}}{2} \right) + E_{sc} A_{sc} \varepsilon_{c,ps} \left( \frac{c_{ps} - d'}{c_{ps}} \right) (d - d') + 2A_p \sigma_{p,ps} d'' \quad (23)$$

163 where  $d''$  is the distance from the center of the compression block of the steel plate to the tension steel.

164 The depth of the compression zone ( $c_{ps}$ ) and strain of concrete ( $\varepsilon_{c,ps}$ ) in the post-stressing stage can be  
165 obtained by solving Eqs. (7), (8), (22) and (23).

166



167 **Ultimate Load Capacity**

168 Assuming that the compression steel has been yielded, the equilibrium equation can be obtained from  
 169 the sum of the internal forces.

$$170 \quad P_u = \alpha\beta b(c_u - 2d_b)f'_c + A_{sc}f_{scy} - A_{st}f_{st} + 2P_{pcu} - 2P_{ptu} \quad (24)$$

171 The equation obtained from taking moments about the tension steel is

$$172 \quad P_u e' = \alpha\beta b(c_u - 2d_b)f'_c \left(d - \frac{\beta c_u}{2}\right) + A_{sc}f_{scy}(d - d') + 2P_{pcu}d_{pcu} - 2P_{ptu}d_{ptu} \quad (25)$$

173 where  $f_{scy}$  is the compression steel yield strength,  $f_{st}$  is the stress in the tension steel,  $P_{pcu}$  and  $P_{ptu}$  are  
 174 the forces defined in Fig. 4(c), and  $d_{pcu}$  and  $d_{ptu}$  are the distances from the center of force  $P_{pcu}$  and  
 175 force  $P_{ptu}$  to the tension steel, respectively.

176 Force  $P_{pcu}$  at the ultimate load is

$$177 \quad P_{pcu} = t_p f_{py} c_{pu} \quad (26)$$

178 where  $t_p$  is the thickness of plate,  $f_{py}$  is the yield strength of steel plate, and  $c_{pu}$  is the depth of the  
 179 neutral axis measured from the extreme compression fiber of the steel plate, as shown in Fig. 4(b),  
 180 which can be calculated by

$$181 \quad c_{pu} = \begin{cases} h & (\text{Case1, } c_{pu} \geq h) \\ (\varepsilon_{cu} - \varepsilon_{c,ps} + \varepsilon_{p,ps})/\phi & (\text{Case2, } c_{pu} < h) \end{cases} \quad (27)$$

182 where  $h$  is the width of steel plate and  $\phi$  is the change of curvature of RC column between the post-  
 183 stressing stage and the ultimate load stage, which can be expressed as

$$184 \quad \phi = \phi_2 - \phi_1 = \frac{\varepsilon_{cu}}{c_u} - \frac{\varepsilon_{c,ps}}{c_{ps}} \quad (28)$$

185 where  $\phi_1$  is the curvature of RC column at the post-stressing stage and  $\phi_2$  is the curvature of the RC  
 186 column at the ultimate load stage, as shown in Fig. 4(a).

187 According to the assumption of curvature compatibility between the RC column and steel plates, the  
 188 force  $P_{ptu}$  is

$$189 \quad P_{ptu} = t_p E_p \left(h - \frac{\varepsilon_{cu} - \varepsilon_{c,ps} + \varepsilon_{p,ps} - \varepsilon_{py}}{\phi}\right) \left[\varepsilon_{py} - \left(\frac{\varepsilon_{cu} - \varepsilon_{c,ps} + \varepsilon_{p,ps}}{\phi} - h\right)\phi\right] \quad (29)$$

190 The depth of the compression zone ( $c_u$ ) and ultimate load-carrying capacity ( $P_u$ ) can be obtained from  
191 Eqs. (7), (8), (24) to (29). If a tension failure occurs, the tension steel yields, and Eq. (24) applies with  
192  $f_{st}=f_{sty}$ .

193  
194

## 195 **A Brief Description of Experimental Study**

196 Because the detailed experimental procedure for preloaded RC columns strengthened with  
197 precambered steel plates subjected to eccentric loading has been presented in our companion paper  
198 (Wang and Su 2012), only a brief description of the test procedure is given in this paper. The new  
199 experimental results on ductility and moment-curvature response of eight precambered steel plate-  
200 strengthened column specimens, involving a new specimen ESC3-3, are presented.

201 All the tested concrete columns have the same dimensions and reinforcement arrangements. Fig. 5  
202 shows the reinforcement and steel plate details. Specimens ESC1-1, ESC2-1 and ESC3-1 were control  
203 specimens without any strengthening measures to demonstrate the structural performance of RC  
204 columns prior to strengthening. The other five specimens were strengthened by precamber steel plates  
205 with varying initial precamber and plate thicknesses. Table 1 shows the average concrete cube and  
206 cylinder compressive strengths ( $f_{cu}$  and  $f_c'$ ) as well as the design parameters for each specimen. Table 2  
207 summarizes the material properties of the steel reinforcements and steel plates. All plate-strengthened  
208 columns were subjected to preloading before the plates were flattened, which was equal to 30% of the  
209 ultimate axial load capacity of the corresponding control column. For the plate-strengthened  
210 specimens, the axial load was applied under a force control with a loading rate of 2 kN/sec. After  
211 tightening the bolts and flattening the precambered plates, the applied load was changed to a  
212 displacement control with a displacement rate of 0.5 mm/min. The test was terminated when the post-  
213 peak load reached 80% of the peak load.

214 Before installing the steel plates, 65 mm × 65 mm steel angles were welded to both ends of the  
215 plates, as shown in Fig. 6. The gaps between the steel angles and the concrete at the bottom and top of  
216 the steel plates were filled with an injection plaster, forming a layer of bedding between the steel

217 angles and the concrete. The post-stress procedure described in Wang and Su (2012), which can avoid  
218 warping or buckling of the steel plates during decompression of the RC column by flattening the  
219 precambered steel plates, was adopted.

220

## 221 **Results and Discussion**

### 222 *Ultimate Load Capacity and Bending Strength*

223 Table 3 summarizes the ultimate axial load capacities of all of the specimens. Compared with the  
224 control column in each of the groups, the strengthened specimens show various degrees of  
225 strengthening from 13.9% to 64.0%. In group A, the ultimate load capacities of Specimens ESC1-2,  
226 ESC1-3 and ESC1-4 are increased by 27.1%, 64.0% and 44.6%, respectively. In group B, the ultimate  
227 load capacity of Specimen ESC2-2 is enhanced by 13.9%. In group C, the ultimate capacity of  
228 Specimen ESC3-3 is increased by 49.0%.

229 According to the proposed theoretical model described in the previous sections, the predicted axial  
230 load capacity ( $P_{pre}$ ) of the specimens was determined by Eq. (22) and Eq. (23). During the calculations  
231 of the ultimate load capacity of the RC columns, the extreme fiber compression strain of concrete  $\varepsilon_{cu}$   
232 was assumed to be 0.003 (Park and Paulay, 1975), and the gross sectional area of the concrete ( $A_c$ ) did  
233 not include the areas of the bolt holes. The predicted axial load capacity of the specimens is presented  
234 in Table 3. Comparing the theoretical and experimental axial load capacities reveals that the proposed  
235 design procedure is generally able to conservatively estimate the actual axial load capacities of the  
236 plate-strengthened columns under eccentric compression loading with an average overestimation of  
237 2.1%.

238 Due to the eccentricity of the applied axial load, a bending moment is always generated. The  
239 ultimate moment ( $M_u$ ) at the mid-height of the column is composed of the primary moment ( $M_p$ ),  
240 which is calculated based on the nominal eccentricity, and the secondary moment ( $M_s$ ) caused by the  
241  $P-\Delta$  effect; both are summarized in Table 3. The definitions of the primary, secondary and ultimate  
242 moments can be found in Wang and Su (2012). In Group A, the secondary moment of the

243 strengthened columns ESC1-2, ESC1-3 and ESC1-4 due to the  $P$ - $\Delta$  effect increased by 27.6%, 49.2%  
244 and 37.3%, respectively. In Group B, the secondary moment of the strengthened column due to the  $P$ -  
245  $\Delta$  effect increased by 24.9%. In Group C, the secondary moment of the strengthened column due to  
246 the  $P$ - $\Delta$  effect increased by 188.3%. It is evident that the bending moment of Specimen ESC3-3 is the  
247 largest among the eight specimens due to the largest lateral displacement and degree of eccentricity as  
248 listed in Table 3.

### 249 ***Deformation and Ductility***

250 The deformability factor ( $\lambda$ ), proposed by De Luca et al. (2011), was adopted to evaluate the  
251 deformation performance of the strengthened columns, which is defined as

$$252 \quad \lambda = \Delta_f / \Delta_u \quad (30)$$

253 where  $\Delta_u$  is the axial shortening at the ultimate load and  $\Delta_f$  is the axial shortening at the failure load,  
254 which is equal to 75% of the ultimate load. In Group A, compared to the control column, the axial  
255 shortening at the failure load of the strengthened columns ESC1-2, ESC1-3 and ESC1-4 improved by  
256 61.7%, 160.2% and 103.9% respectively, as shown in Fig. 7(a), and the deformability factor of the  
257 strengthened columns increased by 27.3%, 61.4% and 65.9% respectively. In Group B, compared to  
258 the control column, the axial shortening at the failure load of the strengthened column improved by  
259 49.0%, as shown in Fig. 7(b), and the deformability factor of the strengthened column increased by  
260 31.8%. In Group C, compared to the control column, the axial shortening at the failure load of the  
261 strengthened column improved by 222.2%, as shown in Fig. 7(c), and the deformability factor of the  
262 strengthened column increased by 93.0%. Thus, the plate thickness plays an important role in  
263 increasing the deformability of the strengthened columns, whereas the initial precamber and  
264 eccentricity do not have a substantial effect on the displacement ductility of columns.

265 The displacement ductility factor ( $\eta$ ) is introduced to evaluate the ductility performance of the  
266 strengthened columns. The load-axial shortening responses of the specimens shown in Fig. 7 can be  
267 idealized as a bi-linear curve (Fig. 8). The displacement ductility factor (Su et al. 2010) is defined as  
268 the ratio of the axial shortening at peak load ( $\Delta_u$ ) to the notional yield displacement ( $\Delta_y$ ); thus,

269

$$\eta = \Delta_u / \Delta_y \quad (31)$$

270 As shown in Table 4, the displacement ductility factors range from 1.36 (for Specimen ESC2-1) to  
 271 1.94 (for Specimen ESC3-3). For each of the groups, the displacement ductility factor of the control  
 272 columns was the lowest. Compared with Specimens ESC1-4 ( $\delta = 6$  mm), the displacement ductility  
 273 factor of Specimens ESC1-3 ( $\delta = 10$  mm) was increased by only 3.4%. Hence, the increase in the  
 274 initial precamber cannot effectively enhance the displacement ductility. Compared with Specimens  
 275 ESC1-2 and ESC1-3 ( $e = 30$  mm), the displacement ductility factors of Specimens ESC2-2 ( $e = 70$   
 276 mm) and ESC3-3 ( $e = 100$  mm) were increased by only 1.4% and 5.4%, respectively. Hence, the  
 277 displacement ductility is not sensitive to the eccentricity of the applied load. Using thicker plates ( $t_p =$   
 278 6 mm) for Specimen ESC1-3 instead of thinner plates ( $t_p = 3$  mm) for Specimens ESC1-2, the  
 279 displacement ductility of ESC1-3 was increased by 30.5 %. Hence, using thicker plates can effectively  
 280 improve the ductility of strengthened columns.

281

### 282 ***Moment-curvature Responses***

283 Fig. 9(a) and Fig. 9(b) show the effects of eccentricity on the moment-curvature relationship of the  
 284 columns. For the specimens strengthened by 3 mm plates, the moment-curvature relationship of  
 285 Specimen ESC2-2 under 70 mm eccentricity was elastic until the moment reached 13.1 kNm, which  
 286 was 19.3% larger than the moment of Specimen ESC1-2 under 30 mm eccentricity. Specimen ESC2-2  
 287 failed when the curvature was  $26.2 \times 10^{-3} \text{ m}^{-1}$ , which was 12.9% larger than that of Specimen ESC1-2.  
 288 For the specimens strengthened by 3 mm plates, the moment-curvature relationship of Specimen  
 289 ESC3-3 under 100 mm eccentricity was elastic until the moment reached 27.2 kNm, which was 97.1%  
 290 larger than the moment of Specimen ESC1-3 under 30 mm eccentricity. Specimen ESC3-3 failed  
 291 when the curvature was  $38.3 \times 10^{-3} \text{ m}^{-1}$ , which was 13.7% larger than that of Specimen ESC1-3.

292 Fig. 9(c) shows the effects of the plate thickness on the moment-curvature relationship of the  
 293 columns. Under the condition of 30 mm eccentricity, the moment-curvature relationship of Specimen  
 294 ESC1-3 strengthened by the plates that were 6 mm thick was elastic until the moment and curvature

295 reached 13.8 kNm and  $5.8 \times 10^{-3} \text{ m}^{-1}$ , respectively, which were 21.1% and 99.7% larger than the  
296 moment and curvature of Specimen ESC1-2 strengthened by the plates that were 3 mm thick.  
297 Specimen ESC1-3 failed when the ultimate curvature was  $32.3 \times 10^{-3} \text{ m}^{-1}$ , which was 38.1% larger than  
298 that of Specimen ESC1-2.

299 Fig. 9(d) shows the effects of the initial precamber on the moment-curvature relationship of the  
300 columns. The moment-curvature relationship of Specimen ESC1-3 with 10 mm initial precamber was  
301 elastic until the moment reached 13.8 kNm, which was 8.7% larger than that of Specimen ESC1-4  
302 with 6 mm initial precamber. Both of them had the same curvature ( $5.7 \times 10^{-3} \text{ m}^{-1}$ ) during the elastic  
303 stage. Specimen ESC1-3 failed when its curvature was  $32.3 \times 10^{-3} \text{ m}^{-1}$ , which was 4.5% larger than that  
304 of Specimen ESC1-4. The results demonstrated that the ductility of the column was mainly affected by  
305 the plate thickness rather than the eccentricity and the initial precamber, and a larger plate thickness  
306 can provide better ductility.

### 307 **Comparison with Available Experimental Results**

308 Montuori and Piluso (2009) tested eight RC columns strengthened with steel cages subjected to  
309 eccentric compression loads. The steel cage consisted of steel angles and battens. The strengthened  
310 columns can be divided into three different types according to the function of steel angles. The  
311 ultimate capacity of the strengthened columns was evaluated using the proposed theoretical model.  
312 The stress-strain relationship of confined concrete used by Montuori and Piluso (2009) was adopted in  
313 our theoretical calculation.

314 Table 5 compares the ultimate load capacity presented in Montuori and Piluso (2009) with that  
315 obtained from the theoretical model. As shown in the table, all the theoretical load capacities ( $P_{pred}$ )  
316 agree well with the experimental ultimate load capacities ( $P_{Mon,exp}$ ). The average discrepancy of  
317  $P_{Mon,exp}/P_{pred}$  is only 2%. Meanwhile, comparing the theoretical results ( $P_{Mon,pred}$ ) proposed by  
318 Montuori and Piluso (2009) with the theoretical results obtained from our proposed model, the average  
319 discrepancy of  $P_{Mon,pre}/P_{pred}$  is also 2%. Hence, the proposed theoretical model is of a similar accuracy  
320 when compared with that from Montuori and Piluso (2009).

## 321 **Conclusions**

322 The paper presents a study on the strengthening of RC columns using precambered steel plates. The  
323 theoretical and experimental findings are summarized as follows:

324 (1) The experimental results show that precambered plates can share the existing axial load in the  
325 original column. Stress-lagging effects can be alleviated by controlling the initial precambered profile  
326 of the steel plates.

327 (2) External steel plates can considerably enhance the axial strength and deformation capacity of  
328 plate-strengthened columns under eccentric compression loading.

329 (3) Thicker steel plates and larger initial precamber can enhance the ultimate load capacity of  
330 columns, and a larger plate thickness can also improve the axial deformation capacity and ductility of  
331 columns significantly.

332 (4) The bending moment capacity of a column is significantly affected by the degree of eccentricity  
333 because the larger degree of eccentricity can increase the lateral displacement at the mid-height of  
334 columns and, hence, increase the secondary moment caused by the  $P-\Delta$  effect.

335 (5) An original theoretical model was developed based on the principles of force equilibrium and  
336 the displacement compatibility between the steel plates and the RC column. The experimental and  
337 theoretical results showed a good agreement with each other. The comparison between the available  
338 test results of Montuori and Piluso (2009) and the predicted theoretical results was also presented. This  
339 study demonstrates that the theoretical model is able to accurately predict the axial load-carrying  
340 capacity of the plate-strengthened columns under eccentric compression loading.

341

## 342 **Acknowledgements**

343 The research described here was supported by the Research Grants Council of the Hong Kong SAR  
344 (Project No. HKU7166/08E) and The University of Hong Kong through Small Project Funding 2010-  
345 2011.

346  
347

348 **References**

- 349 Adam, J.M., Ivorra, S., Gimenez, E., Moragues, J.J., Miguel, P., Miragall, C. and Calderon, P.A.  
350 (2007). "Behaviour of axially loaded RC columns strengthened by steel angles and strips." *Steel*  
351 *and Composite Structures*, 7(5), 405-419.
- 352
- 353 Adam, J.M., Gimenez, E., Calderon, P.A., Pallarés, F.J. and Ivorra, S. (2008). "Experimental study of  
354 beam-column joints in axially loaded RC columns strengthened by steel angles and strips." *Steel*  
355 *and Composite Structures*, 8(4), 329-342.
- 356
- 357 Adam, J.M., Ivorra, S., Pallares, F.J., Gimenez, E. and Calderon, P.A. (2008). "Column-joint assembly  
358 in RC columns strengthened by steel caging." *Proc. ICE - Structures and Buildings*, 161(6), 337-  
359 348.
- 360
- 361 Adam, J.M., Ivorra, S., Pallares, F.J., Gimenez, E. and Calderon, P.A. (2009). "Axially loaded RC  
362 columns strengthened by steel caging: Finite element modeling." *Construction and Building*  
363 *Materials*, 23(6), 2265-2276.
- 364
- 365 Adam, J.M., Ivorra, S., Pallares, F.J., Gimenez, E. and Calderon, P.A. (2009). "Axially loaded RC  
366 columns strengthened by steel caging." *Proc. ICE - Structures and Buildings*, 162(3), 199-208.
- 367
- 368 Cirtek, L. (2001). "RC columns strengthened with bandage – experimental programme and design  
369 recommendations." *Construction and Building Materials*, 15(8), 341–349.
- 370
- 371 Collins, M.P. and Mitchell, D. (1987) *Prestressed Concrete Structures*, Prentice Hall, Englewood  
372 Cliffs.
- 373
- 374 De Luca, A., Nardone, F., Matta, F., Nanni, A., Liqola, G. and Prota, A. (2011). "Structural  
375 evaluation of full-scale FRP-confined reinforced concrete columns." *Journal of Composites for*  
376 *Construction*, 15(1), 112-123.
- 377
- 378 Ersoy, U., Suleiman, R. and Tankut, T. (1993). "Behavior of jacketed columns." *ACI Structural*  
379 *Journal*, 90(3), 288-293.
- 380
- 381 Frangou, M., Pilakoutas, K. and Dritsos, S. (1995). "Structural repair/strengthening of RC Columns." *Construction and Building Materials*, 9(5), 259-266.
- 382
- 383
- 384 Fukuyama, H. and Sugano, S. (2000). "Japanese seismic rehabilitation of concrete buildings after the  
385 Hyogoken-Nanbu Earthquake." *Cement and Concrete Composites*, 22(1), 59-79.
- 386
- 387 Garzón-Roca, J., Adam, J.M. and Calderón, P.A. (2011). "Behaviour of RC columns strengthened by  
388 steel caging under combined bending and axial loads." *Construction and Building Materials*, 25(5),  
389 2402-2412.
- 390
- 391 Garzón-Roca, J., Ruiz-Pinilla, J., Adam, J.M. and Calderón, P.A.(2011). "An experimental study on  
392 steel-caged RC columns subjected to axial force and bending moment." *Engineering Structures*,  
393 33(2), 580-590.
- 394
- 395 Giménez, E., Adam, J.M., Ivorra, S. and Calderón, P.A. (2009). "Influence of strips configuration on  
396 the behaviour of axially loaded RC columns strengthened by steel caging and strips." *Materials*  
397 *and Design*, 30(10), 4103-4111.
- 398



- 399 Giménez, E., Adam, J.M., Ivorra, S., Moragues, J.J., and Calderón, P.A. (2009). "Full-scale testing of  
400 axially loaded RC columns strengthened by steel angles and strips." *Advances in Structural*  
401 *Engineering*, 12(2), 169-181.  
402
- 403 Hognestad, E., Hanson, N., McHenry, D. (1955). "Concrete stress distribution in ultimate strength  
404 design." *ACI Structural Journal*, 52(6), 455-479.
- 405
- 406 Li, J., Gong, J. and Wang, L. (2009). "Seismic behavior of corrosion-damaged reinforced concrete  
407 columns strengthened using combined carbon fiber-reinforced polymer and steel jacket."  
408 *Construction and Building Materials*, 23(7), 2653-2663.  
409
- 410 Montuori, R. and Piluso, V. (2009). "Reinforced concrete columns strengthened with angles and  
411 battens subjected to eccentric load." *Engineering Structures*, 31(2), 539-550.
- 412
- 413 Oey, H.S. and Aldrete, C.J. (1996). "Simple method for upgrading an existing reinforced-concrete  
414 structure." *Practice Periodical on Structural Design and Construction*, 1(1), 47-50.  
415
- 416 Ramírez, J.L. (1966). "Ten concrete column repair methods." *Construction and Building Materials*,  
417 10(3), 195-202.  
418
- 419 Su, R.K.L., Cheng, B., Wang, L., Siu, W.H. and Zhu, Y. (2011). "Use of bolted steel plates for  
420 strengthening of reinforced concrete beams and columns", *The IES Journal Part A: Civil &*  
421 *Structural Engineering*, 4(2), 55-68.  
422
- 423 Su, R.K.L., Siu, W.H. and Smith, S.T. (2010). "Effects of bolt-plate arrangements on steel plate  
424 strengthened reinforced concrete beams." *Engineering Structures*, 32(6), 1769-1778.
- 425
- 426 Su, R.K.L., and Wang, L. (2012). "Axial strengthening of preloaded rectangular concrete columns by  
427 precambered steel plates." *Engineering Structures*, (Article in press).
- 428
- 429 Park, R., and Paulay, T. (1975) *Reinforced Concrete Structures*, John Wiley & Sons, New York.  
430
- 431 Takeuti, R.A., de Hanai, J.B. and Mirmiran, A. (2008). "Preloaded RC columns strengthened with  
432 high-strength concrete jackets under uniaxial compression." *Materials and Structures*, 41(7),  
433 1251-1262.  
434
- 435 Wang, L. and Su, R.K.L. (2012). "Experimental investigation of preloaded RC columns strengthened  
436 with precambered steel plates under eccentric compression loading." *Advances in Structural*  
437 *Engineering*, (Article in press).  
438
- 439 Wu, Y.F., Liu, T. and Oehlers, D.J. (2006). "Fundamental principles that govern retrofitting of  
440 reinforced concrete columns by steel and FRP jacketing." *Advances in Structural Engineering*,  
441 9(4), 507-533.  
442  
443  
444  
445

446  
447

**Table 1.** Summary of strengthening details

Group	Specimen	$f_{cu}$ (MPa)	$f'_c$ (MPa)	$E_c$ (GPa)	$L_{rc}$ (mm)	$e$ (mm)	$t_p$ (mm)	$\delta$ (mm)	$P_{pl}$ (kN)
[A]	ESC1-1	31.3	25.6	23.8	600	30	-	-	-
	ESC1-2	31.9	25.8	23.9	600	30	3	10	101
	ESC1-3	31.6	25.9	23.9	600	30	6	10	101
	ESC1-4	32.7	26.1	24.0	600	30	6	6	101
[B]	ESC2-1	33.3	27.8	24.8	600	70	-	-	-
	ESC2-2	32.0	25.7	23.8	600	70	3	10	63
[C]	ESC3-1	29.7	24.2	23.1	600	100	-	-	-
	ESC3-3	32.6	26.5	24.2	600	100	6	10	43

448  
449  
450

**Table 2.** Material properties of reinforcements and steel plates

Steel Plate		
Thickness	$f_{yp}$ (MPa)	$E_p$ (GPa)
3 mm	301	215
6 mm	327	219

Reinforcement bars		
Specimen	$f_y$ (MPa)	$E_s$ (GPa)
T10	497	198
T12	516	198
R6	464	186
R8	437	187

451

452  
453  
454

**Table 3.** Comparison of the theoretical and experimental results

Group	Specimen	$\zeta_u$ (mm)	$M_p$ (kN m)	$M_s$ (kN m)	$M_u$ (kN m)	$P_{exp}$ (kN)	$P_{pred}$ (kN)	$P_{exp}/P_{pred}$
[A]	ESC1-1	5.51	10.08	1.85	11.93	336	329	1.02
	ESC1-2	5.53	12.81	2.36	15.17	427	390	1.09
	ESC1-3	5.01	16.53	2.76	19.29	551	545	1.01
	ESC1-4	5.23	14.58	2.54	17.12	486	471	1.03
[B]	ESC2-1	9.62	14.63	2.01	16.64	209	208	1.01
	ESC2-2	10.55	16.66	2.51	19.17	238	227	1.05
[C]	ESC3-1	10.11	14.30	1.45	15.75	143	143	1.00
	ESC3-3	17.36	24.10	4.18	28.28	213	222	0.96

455  
456

*Note:*  $P_{exp}$  is the test result,  $P_{pred}$  is the predicted result.

457

458

**Table 4.** Summary of deformability and ductility factors

Group	Specimen	$\Delta_y$ (mm)	$\Delta_u$ (mm)	$\Delta_f$ (mm)	$\lambda$	$\eta$
[A]	ESC1-1	0.71	0.97	1.28	1.32	1.37
	ESC1-2	0.87	1.23	2.07	1.68	1.41
	ESC1-3	0.85	1.56	3.33	2.13	1.84
	ESC1-4	0.67	1.19	2.61	2.19	1.78
[B]	ESC2-1	0.28	0.38	0.49	1.29	1.36
	ESC2-2	0.30	0.43	0.73	1.70	1.43
[C]	ESC3-1	0.14	0.21	0.27	1.29	1.50
	ESC3-3	0.18	0.35	0.99	2.83	1.94

459

460

461

462

**Table 5.** Comparison of ultimate load capacities from Montuori and Piluso (2009) and the present proposed theoretical model

Specimen	$P_{Mon,exp}$ (kN)	$P_{Mon,pred}$ (kN)	$P_{pred}$ (kN)	$P_{Mon,exp}/P_{pred}$	$P_{Mon,pred}/P_{pred}$
A-R1	513.95	527.02	507.08	1.01	1.04
B-R1a	703.23	683.62	683.38	1.03	1.03
B-R1b	662.71	649.75	656.56	1.01	0.99
C-R1	498.74	495.15	480.55	1.04	1.03
D-R1	545.19	553.24	528.23	1.03	1.05
D-R2	568.98	583.22	563.18	1.01	1.04
D-R3	483.63	453.84	462.86	1.04	0.98
E-R1	713.24	713.80	705.28	1.01	1.01
Mean	-	-	-	1.02	1.02

463

*Note:*  $P_{Mon,exp}$  is the test result and  $P_{Mon,pred}$  is the predicted result, both from Montuori and Piluso (2009).

464

465

466

467 **A List of Figure Captions**

468 Figure 1. The configuration of the proposed strengthening method

469 Figure 2. Stress-block factors

470 Figure 3. Lengths and deformations of RC column and steel plates at various loading stages

471 Figure 4. Strain distribution and calculation; (a) Concrete strain distribution; (b) Steel plate strain  
472 distribution; (c) Steel plate stress distribution in the theoretical calculation

473 Figure 5. Reinforcement and precambered steel plates; (a) RC details; (b) Steel plate details

474 Figure 6. Joint at the end of precambered steel plates; (a) Anchor bolts details; (b) Steel angle details

475 Figure 7. Load-axial shortening curves; (a) Group A; (b) Group B; (c) Group C

476 Figure 8. Definition of displacement ductility factor

477 Figure 9. Moment-curvature responses of columns; (a)  $t_p=3$  mm,  $\delta=10$  mm; (b)  $t_p=6$  mm,  $\delta=10$  mm; (c)  
478  $e=30$  mm,  $\delta=10$  mm; (d)  $t_p=6$  mm,  $e=30$  mm

479

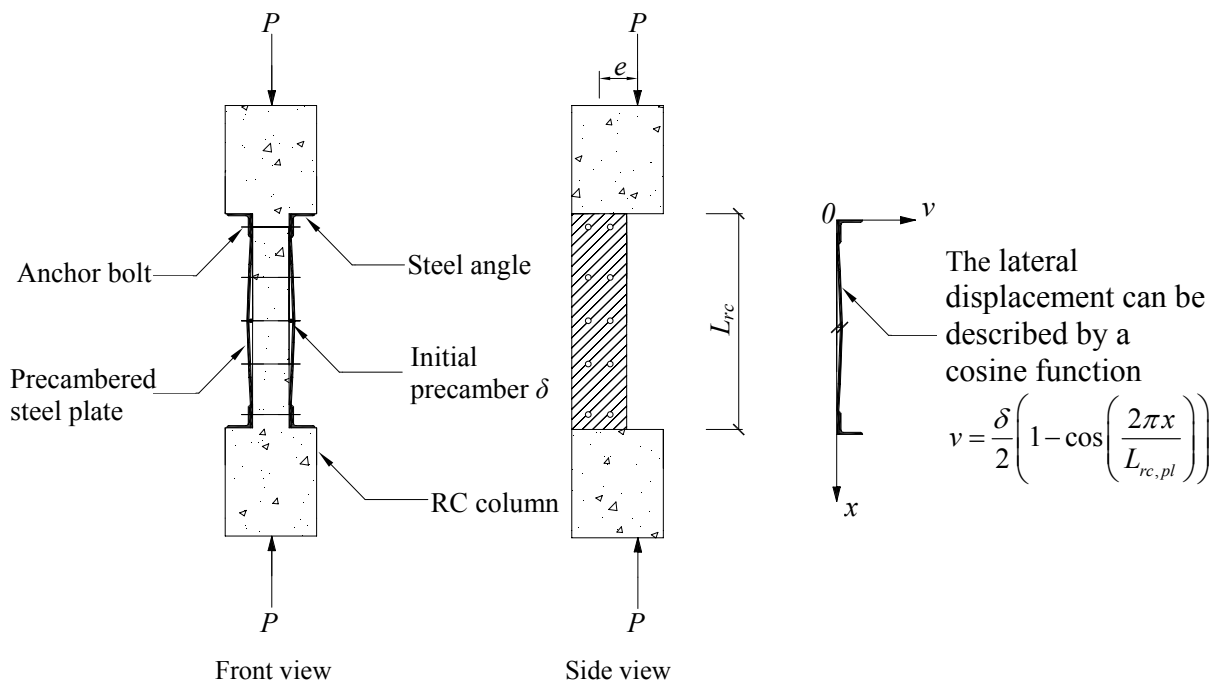


**Fig. 1.** The configuration of the proposed strengthening method

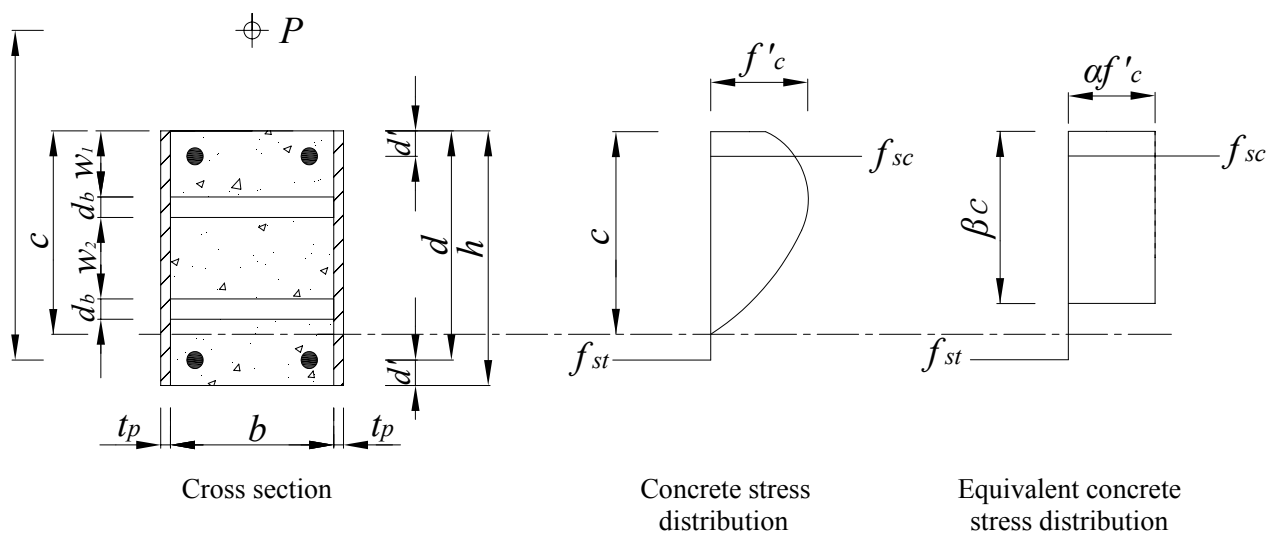


**Fig. 2.** Stress-block factors

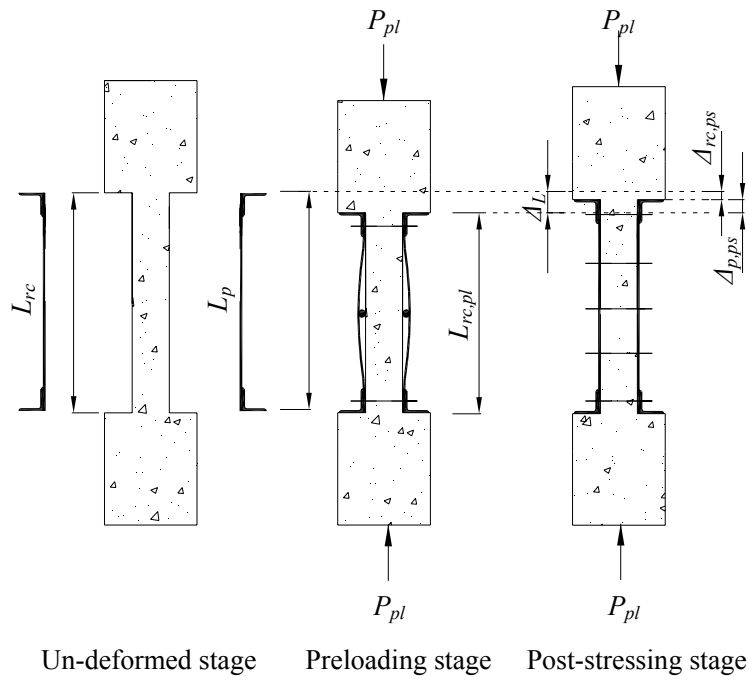


**Fig. 3.** Lengths and deformations of RC column and steel plates at various loading stages

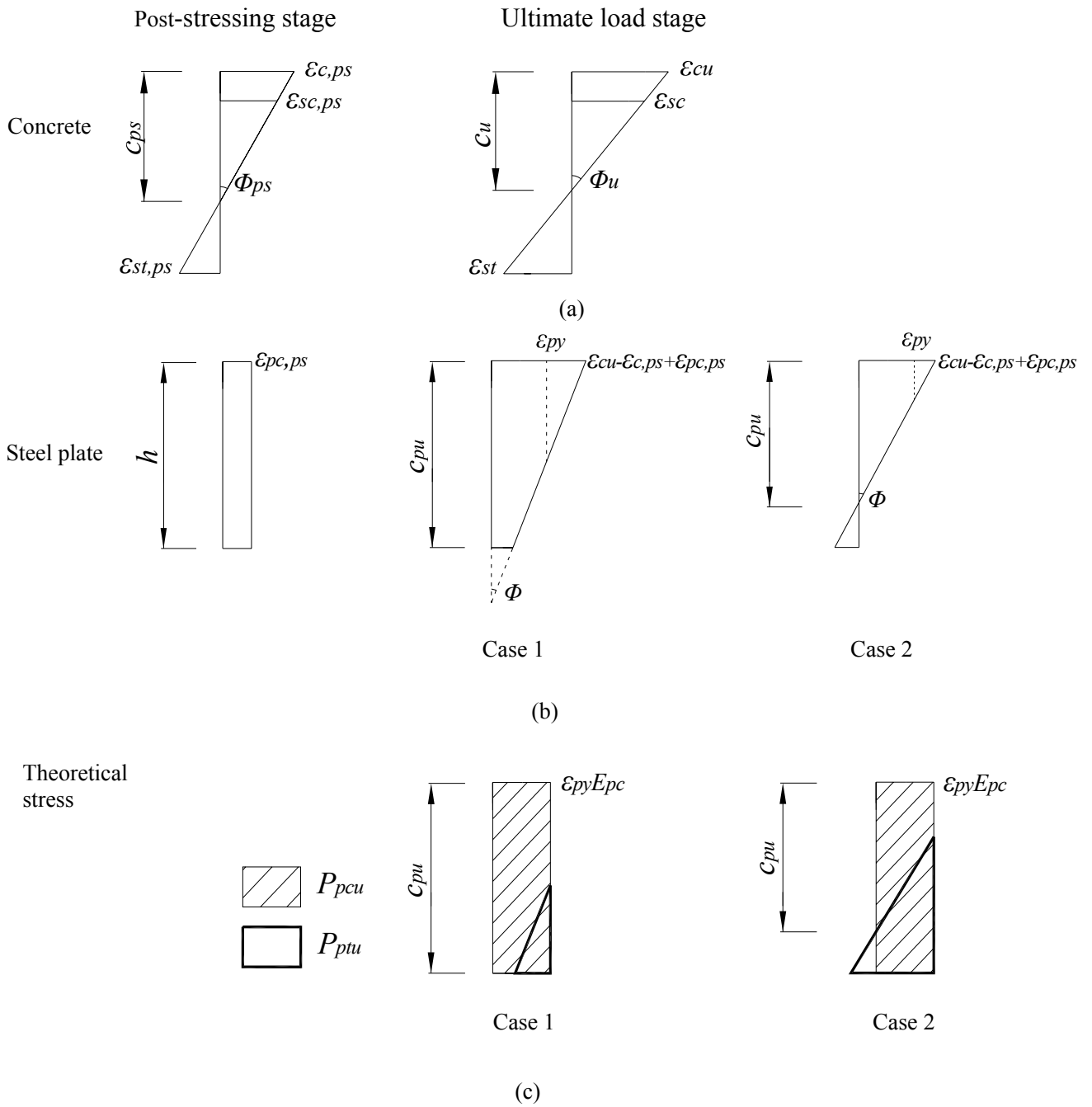


**Fig. 4.** Strain distribution and calculation; (a) Concrete strain distribution; (b) Steel plate strain distribution; (c) Steel plate stress distribution in the theoretical calculation

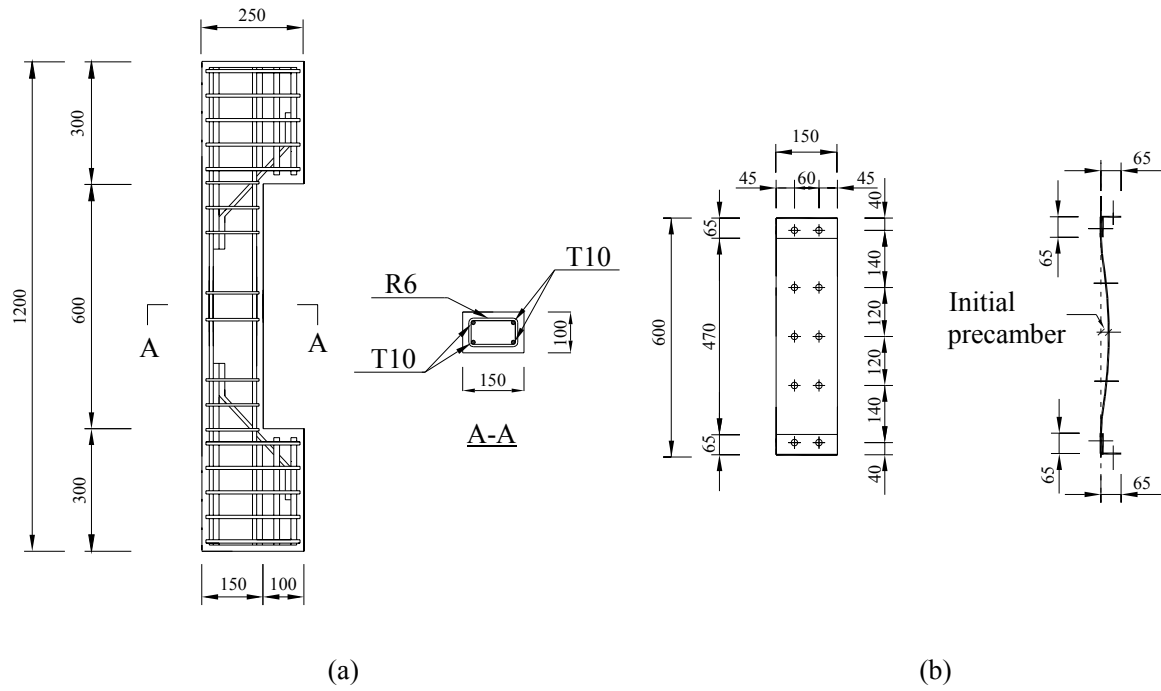


**Fig. 5.** Reinforcement and precambered steel plates; (a) RC details; (b) Steel plate details

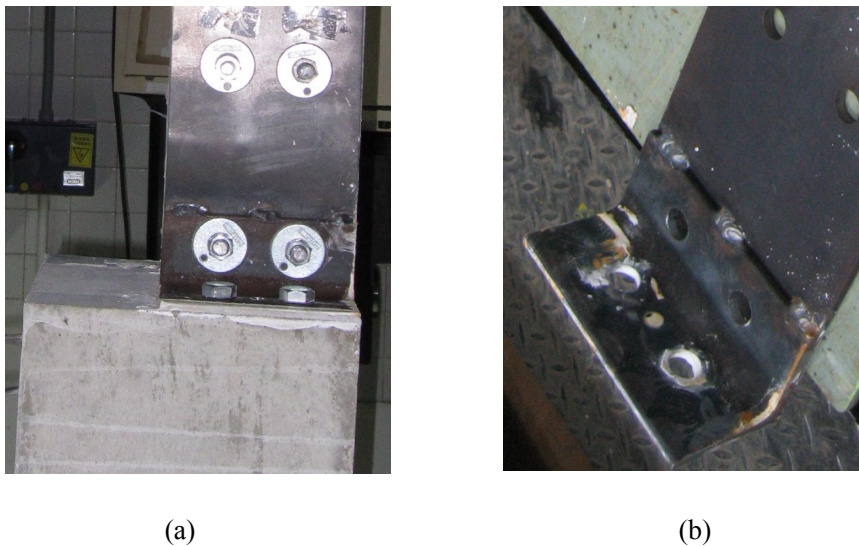
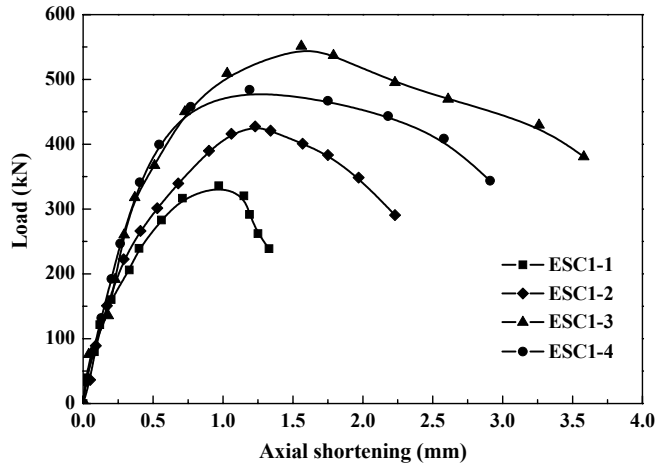
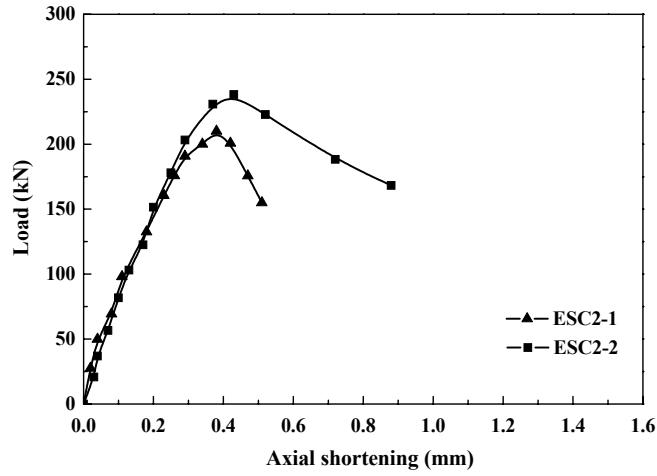


**Fig. 6.** Joint at the end of precambered steel plates; (a) Anchor bolts details; (b) Steel angle details

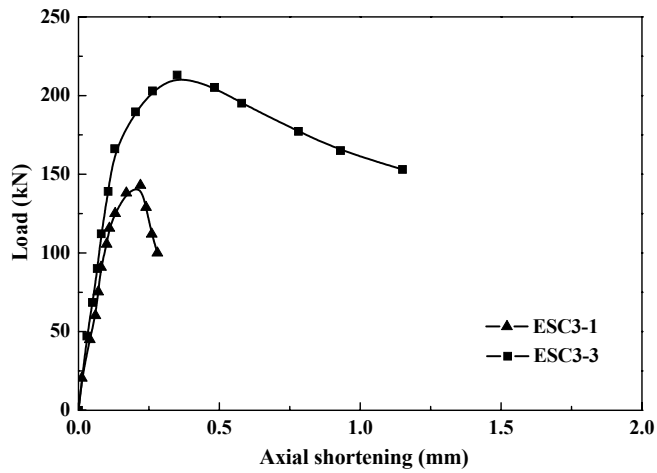




(a)



(b)



(c)

**Fig. 7.** Load-axial shortening curves; (a) Group A; (b) Group B; (c) Group C

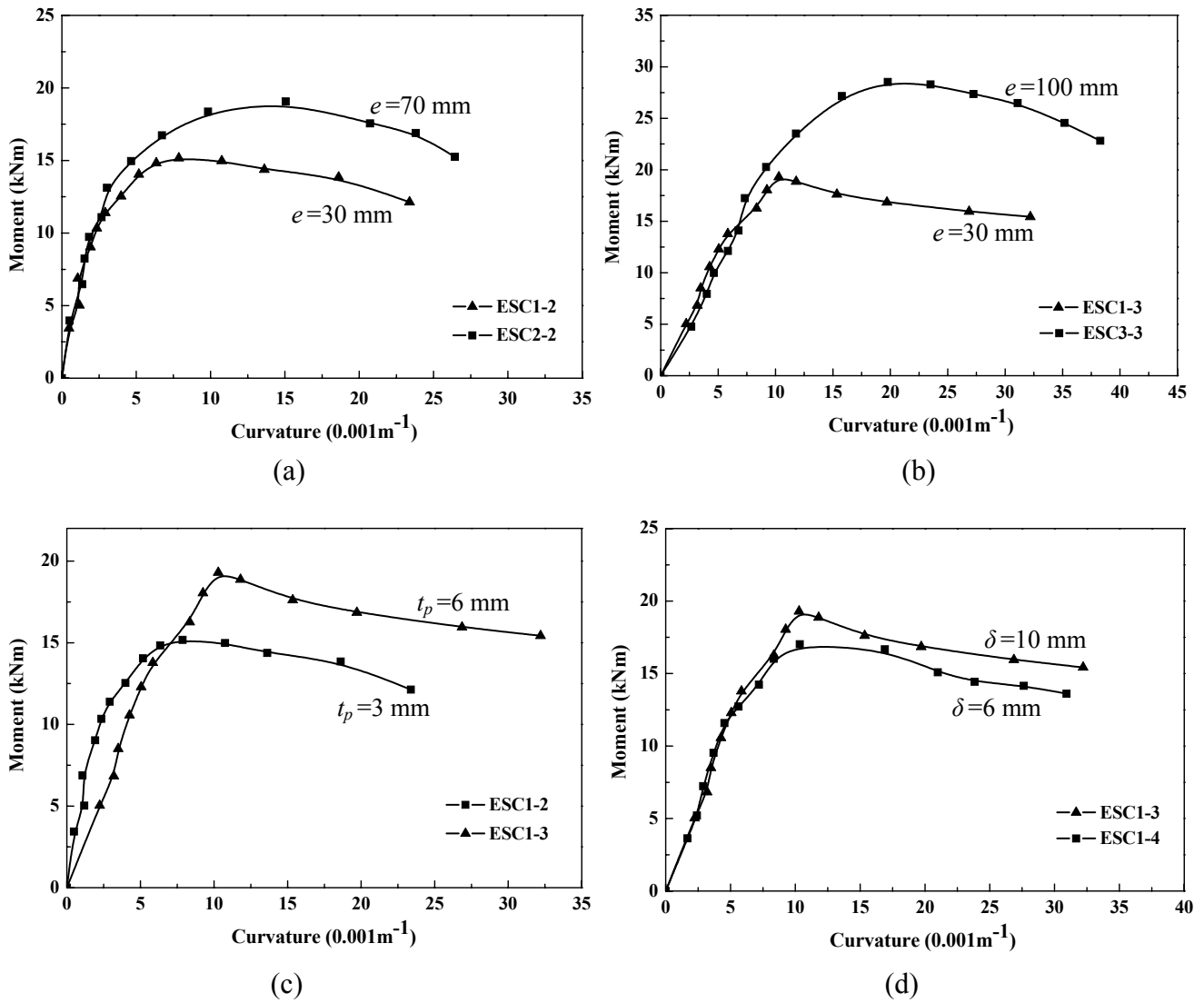


**Fig. 8.** Moment-curvature responses of columns; (a)  $t_p=3$  mm,  $\delta=10$  mm; (b)  $t_p=6$  mm,  $\delta=10$  mm; (c)  $e=30$  mm,  $\delta=10$  mm; (d)  $t_p=6$  mm,  $e=30$  mm